NACA RM E54G27a

NACA

RESEARCH MEMORANDUM

INVESTIGATION OF SUPERSONIC-COMPRESSOR ROTORS DESIGNED WITH EXTERNAL COMPRESSION

By Lawrence J. Jahnsen and Melvin J. Hartmann

Lewis Flight Propulsion Laboratory
Cleveland, Ohio

[redacted]

NATIONAL ADVISORY COMMITTEE
FOR AERONAUTICS

WASHINGTON
September 24, 1954

[redacted]

NATIONAL ADVISORY COMMITTEE FOR AERONAUTICS

RESEARCH MEMORANDUM

INVESTIGATION OF SUPERSONIC-COMPRESSOR ROTORS DESIGNED WITH EXTERNAL COMPRESSION

By Lawrence J. Jahnsen and Melvin J. Hartmann

SUMMARY

Since the shock-in-rotor type supersonic compressor must reduce the relative velocity to a Mach number of 1.0, the possibility of utilizing the relatively good characteristics of the spike-type diffuser in the supersonic compressor was considered. The principle of the spike-type diffuser (external compression) was applied to a 16-inch compressor rotor. The external compression was to a Mach number of 1.0 in the passage entrance region. With this compressor rotor, the design entrance conditions could not be established. The compressor rotor blade was therefore modified to decrease the external compression and the area contraction ratio. The modified compressor rotor more nearly achieved the design entrance conditions, as indicated by a decrease in deviation from design inlet relative angle from 6.6° for the original rotor to 3.3° for the modified compressor rotor.

The modification to the compressor rotor, which resulted in a somewhat closer approach to the design entrance conditions, resulted in an increase in design-speed maximum total-pressure ratio from 2.20 to 2.27 and in adiabatic efficiency from 0.72 to 0.76. The maximum equivalent weight flow increased from 21.4 to 23.2 pounds per second. An analysis of the off-design performance indicated that in neither configuration was the minimum area utilized effectively. Apparently, flow separation due to the rapid change in direction of the suction surface was encountered in the original rotor. Whereas this change in direction was reduced in the modified rotor, the Mach number at which a normal-shock - boundary-layer interaction was encountered at the off-design value was increased and may have resulted in flow separation.

INTRODUCTION

The design of compressor stages with high flow capacity and high stage pressure ratio results in high inlet axial Mach number and high wheel speed, which combine to give supersonic velocities relative to the rotor blade row. Compressors which utilize relative supersonic velocities are referred to as supersonic compressors. One method of utilizing

these supersonic relative velocities is to decelerate the flow in the rotor passages. Each passage may then be considered a supersonic diffuser. This type of compressor has been referred to as the shock-in-rotor type supersonic compressor.

Initial consideration of shock-in-rotor type supersonic compressors was made by the NACA in reference 1. Experimental performance of several rotors of the shock-in-rotor type was reported in references 2 to 4. The observed performance has generally given pressure ratios of about 2.0 and efficiencies from 0.75 to 0.80 for the rotor alone. The pressure ratios that were attained were considerably below the design value of about 3.0. In addition, the exit flow distribution was generally unsatisfactory.

The failure to approach the design pressure ratio has been attributed in part to the lack of efficient subsonic diffusion. Possible reasons for the lack of diffusion were considered to be a severe redistribution of the flow caused by radial pressure gradients behind the shock and a flow separation caused by a shock - boundary-layer interaction. An investigation in which the unbalanced radial pressure gradients were reduced was conducted (ref. 4). The reduction of radial pressure gradient did not appreciably improve either the subsonic diffusion or the flow distribution. The principle cause of the poor performance was then attributed to separation caused by the shock - boundary-layer interaction.

To reduce the tendency of the flow to separate at the shock - boundary-layer interaction, the Mach number ahead of the shock should be made as close to 1.0 as possible (ref. 5). One method of reducing the Mach number at which the strong shock occurs in the compressor blade passage is to incorporate the spiked-diffuser principle. Besides reducing the Mach number, such a design may be expected to reduce the flow velocity with a relatively high total-pressure recovery. To apply this principle of external compression to compressor blades, the suction surface near the leading edge should be contoured to produce weak compression waves ahead of the rotor passage entrance in a manner analogous to the spike of a spiked diffuser. The design of compressor blading incorporating this principle is considered in reference 6 along with the experimental performance in Freon-12 of a rotor utilizing the spiked-diffuser principle. The design flow conditions into the rotor of reference 6 were not obtained, and the performance showed little if any improvement over previous rotors. The failure to establish the design entrance flow conditions was attributed to the effect of the leading-edge thickness.

The subject rotor was investigated to obtain further information concerning the entrance flow into blading incorporating the spiked-diffuser principle. Experimental performance was obtained with air as the test medium, first with an external wave system designed to give isentropic compression to a Mach number of 1.0 at the passage entrance.

The entrance section of the suction surface was then recontoured to reduce the amount of external compression to values established in reference 6 for the given wedge angle. The modification also incorporated an allowance for the blade leading-edge thickness. This report presents the performance of the two rotor configurations and an analytical investigation of the off-design losses and operation of these configurations.

APPARATUS

Blade Design

The application of the spiked-diffuser principle to the entrance section of a compressor blade is illustrated in figure 1. (Symbols used in this report are defined in appendix A.) The entrance flow direction is determined by the region of the suction surface (a-b), which lies ahead of the Mach line originating on the suction surface and intersecting the leading edge of the following blade (ref. 1). Weak compressions are then formed by contouring the suction surface (b-c) behind this Mach wave (from b to d).

For the design condition of the rotor, a tip speed of 1600 feet per second and a hub-tip radius ratio of 0.75 were selected. The entrance axial Mach number at the tip was selected as 0.73.

The velocity diagrams for the original compressor rotor are given in figure 2. Inlet guide vanes were incorporated in order to obtain simple radial equilibrium for a Mach number of 1.0 in the passage minimum-area section. This resulted in a guide-vane turning variation of 3° to 26° from the rotor tip to hub section. The relative entrance Mach number varied from 1.71 at the rotor tip to 1.61 at the rotor hub section. The design weight flow was 26.77 pounds per second and the design total-pressure ratio was 2.79 with an assumed adiabatic efficiency of 0.85 and with a deficiency in exit area of 10 percent.

With the entrance vector diagram thus determined, the blade entrance shape was obtained by the method of characteristics. The rotor was designed with 29 blades. The suction surface was contoured to obtain isentropic compression to a Mach number of 1.0 at the passage entrance region. Figure 3(a) shows a sketch of the design flow configuration and the blade coordinates at the pitch section. The blades are thickened near the leading edge to obtain the necessary mechanical strength without a large wedge angle (between suction surface and pressure surface). This results in a compression wave and subsequent expansion waves of small magnitude. After the minimum-area region, the suction surface of the blade was faired with an area variation corresponding to a cone of 6° included angle. The blade trailing-edge thickness was 0.025 inch. The blade sections are constructed for the tip, pitch, and hub radii. The blade-section centers of gravity were alined in the radial direction, and the blade surfaces were faired between three sections.

[redacted]

The original compressor rotor was modified by reducing the maximum change in angle of the compression ramp to

$$\varphi = \frac{1}{2}(\nu_1 - \varepsilon)$$

as given in reference 6. The velocity diagram for the modified compressor is given in figure 2, and a sketch of the design flow configuration and the blade coordinates at the pitch section are shown in figure 3(b). The suction surface was altered by removing the thickened portion near the leading-edge section so that from the leading edge to the start of the compression wave system was a straight line (along a-b, fig. 1). The small leading-edge thickness was considered to result in a slight angle of incidence and a corresponding wave system at the leading edge of the rotor blade (not shown on illustration) as indicated in reference 4. In the modification a boundary-layer allowance of 0.010 inch per inch was considered to start at the compression ramp (b-c, fig. 1) and was removed from the blade thickness in constructing the blade profile. The modification of the external wave system resulted in a reduction of relative Mach number from 1.62 to 1.43 at the rotor pitch section. The minimum area was then determined by modifying the isentropic area ratio by the limiting contraction ratio for a Mach number of 1.43. The subsonic portion was then faired to the existing blade section. Blade sections were determined for the hub, pitch, and tip sections of the rotor and were faired radially. The modified configuration resulted in a design flow of 25.64 pounds per second. A photograph of the rotor with the original blades is shown in figure 4.

Variable-Component Test Rig

The compressor test rig of references 7 and 8 was modified so that the compressor rotor could be investigated with air as the test medium. The weight flow was measured by a 21.5-inch thin-plate open-end orifice. The inlet piping system was revised to permit operation of the rotor in refrigerated air from the service system with an adjustable orifice to measure the weight flow. The rotor was driven by a 3000-horsepower variable-frequency motor with a speed control through a speed-increaser gear to provide the design speed of approximately 20,000 rpm. A sketch of the test rig is shown in figure 5.

Instrumentation

The pressure drop over the open-end orifice was measured by a micromanometer, and the inlet temperature was measured by two iron-constantan thermocouples. For that portion of the investigation in which the adjustable orifice was used, the pressure drop was measured with a water U-tube and the inlet temperature was measured by two iron-constantan

thermocouples. The temperature of the inlet depression tank (4 ft in diameter by 6 ft in length) was measured by six iron-constantan thermocouples at the centers of equal annular areas, and the pressure was obtained by the average of four equally spaced static taps.

Survey data were obtained at three axial stations with the instrument probes shown in figure 6. The guide-vane turning was obtained by a minature claw at instrument station 1, located 0.8 inch ahead of the leading edge of the rotor tip as shown on figure 5. The rotor performance was obtained at stations 2 and 3, located distances of 1.6 and 7.25 inches, respectively, behind the rotor-tip trailing edge. Each station had temperature, total-pressure claw, and static-pressure probes (fig. 6). The temperature probes were spike-type iron-constantan thermocouples combined with direction-sensitive pressure tubes or a similar probe including a total-pressure tube. The radial surveys were taken at 10 radial stations with automatic survey actuator equipment.

PROCEDURE

The compressor rotor was operated over a range of speed from 50 to 100 percent design speed. Inlet pressure was maintained between 25 and 28 inches mercury absolute for all runs. The compressor rotor performance was obtained from open throttle to audible surge for each speed by adjusting the discharge throttle. The design speed portion of the rotor performance curves was obtained in refrigerated air to reduce the rotational speed of the rotor. The rotor performance was computed by the survey data at station 3. The computational method was similar to that of reference 3.

EXPERIMENTAL RESULTS

The 16-inch supersonic-compressor rotor with external compression to a Mach number of 1.0 was experimentally investigated over a range of speed from 50 to 100 percent design speed. The over-all performance data (fig. 7(a)) indicated that the weight flow was somewhat lower than the design weight flow and that the performance was relatively poor. Thus, from these over-all data it can be assumed that the design entrance conditions were not established. The compressor rotor was modified as described in a preceding section and operated over the same range of conditions as the original compressor rotor. The data for the two configurations will be presented together in the following section so that the two configurations can be compared as the data are presented.

Over-All Performance

The mass-averaged total-pressure ratio, adiabatic efficiency, and equivalent weight flow are presented in figures 7(a) and (b) for the

original and modified compressor rotors. The original compressor rotor obtained a peak total-pressure ratio of 2.20 and an adiabatic efficiency of 0.72 at the design speed. Modifying the compressor rotor resulted in an increased total-pressure ratio of 2.27 and adiabatic efficiency of about 0.76. The modification also resulted in an increase in maximum equivalent weight flow from 21.4 to 23.2 pounds per second. The modified rotor obtained approximately a 5-percent reduction in weight flow as the back pressure was increased at design speed. Such compressor characteristics have been obtained in other supersonic-compressor rotors (ref. 9) and are attributed to the occurrence of a strong shock ahead of the compressor blade passage.

The rotor characteristic of the shock-in-rotor compressor usually approached a constant weight flow near design speed (refs. 2 to 4). Rotors similar to open-throat convergent-divergent diffusers exhibited this near-vertical characteristic (ref. 1). In this case, forcing a shock ahead of the passage from the minimum section would produce a discontinuity in performance. The rotor in this investigation should follow more closely the characteristic of the spike diffuser, which does not exhibit a discontinuity in performance at the point where the mass flow begins to decrease. Thus, the slight decrease in weight flow was anticipated for this type of supersonic-compressor rotor.

For both rotors the maximum rotor efficiency at each speed was nearly constant, with a slight tendency toward increased efficiency at low speeds. The range of equivalent weight flow increases as the speed is decreased, with the increase in range being slightly larger for the modified compressor rotor.

Inlet Conditions

The measured inlet conditions for the two rotor configurations at the point of highest total-pressure ratio obtained at the maximum weight flow (points A and B of figs. 7(a) and (b)) along with the inlet design conditions are indicated in figure 8. This is considered the point which most closely approaches the design flow configuration. The original compressor rotor operated with a deviation from design relative inlet flow angle of approximately 6.6° at the pitch section. This discrepancy between measured and design values does not change appreciably from hub to tip section. The design relative inlet angle was increased slightly in the modified rotor, and the measured angle is about 3.3° higher than the design value at the rotor pitch section.

The measured inlet axial and relative Mach numbers are indicated in figure 8. The design axial Mach number at the pitch section of the original compressor rotor was 0.72 and the measured value was 0.49. The

modification resulted in a reduction in the design axial Mach number to 0.65 and an increase in observed axial Mach number to 0.53 at the rotor pitch section. The relative inlet Mach number resulting from the inlet flow angle and axial inlet Mach number is also shown in figure 8. The design relative inlet Mach number at the pitch section of the original rotor was about 1.64 compared with a measured value of 1.47. The modification changed the design value to 1.56, and a measured value of 1.50 was obtained. Thus, the values given in figure 8 indicate the large discrepancy between the design and the measured inlet conditions and the fact that the modification described improved slightly the agreement between the design and measured values.

Outlet Conditions

The performance parameters for the two compressor configurations measured at the rotor discharge at design speed and at the point of highest total-pressure ratio obtained at maximum weight flow (points A and B of figs. 7(a) and (b)) are shown in figure 9. The total pressure is the highest for the tip section for both rotors. For the original rotor the total-pressure ratio at the rotor hub section is 1.98 and at the tip section is about 2.17, whereas the modified compressor rotor varies from about 1.99 to about 2.21. The adiabatic efficiency for the original compressor rotor varies from 0.76 near the rotor hub to 0.62 near the rotor tip. The modified compressor rotor obtained an adiabatic efficiency of 0.79 near the hub to 0.64 near the rotor tip. Thus, the modification has resulted in improved performance along the complete rotor blade. The unit mass flow over the compressor radius is indicated in figure 9 for both configurations. Similar to other supersonic-compressor rotors of the shock-in-rotor type, the original rotor indicated a very low unit mass flow at the rotor tip section. The modified compressor rotor obtained a higher weight flow over the entire rotor passage with a larger percentage of the mass flow passed through the rotor tip section.

The relative discharge conditions are shown in figure 10. The relative discharge flow angle for the original compressor rotor varied from about 61.0° to about 77.5°. The excessively high flow angle at the rotor tip is typical of experimental results for shock-in-rotor type supersonic-compressor rotors. The modified rotor shows the same tendency of high relative flow angles at the rotor tip with the measured tip flow angle being about 75°. The modification resulted in very little change in relative flow angle at the hub.

The relative total-pressure recovery for the two configurations is shown in figure 10. For the original compressor rotor the recovery is about 0.84 at the rotor hub section and decreases to about 0.69 at the rotor tip section. The modified rotor configuration resulted in a total-pressure recovery of about 0.84 at the hub and is reduced to about

0.72 at the rotor tip section. Thus, the total-pressure recovery for the two configurations is about the same at the rotor hub section and is improved slightly at the rotor tip section.

The relative discharge Mach number for the two rotor configurations is shown in figure 10. For the original configuration the relative discharge Mach number varies from about 0.75 to about 0.64 from the hub to tip section. The modified rotor obtained a relative discharge Mach number range of about 0.74 to 0.67. Thus, the modified compressor rotor has a relative discharge Mach number slightly higher at the tip section than the original compressor rotor.

DISCUSSION OF RESULTS

Entrance Flow Conditions

The design entrance conditions were not established with the external-compression supersonic-compressor rotors used in this investigation. Similar difficulty was experienced with the compressor rotor of reference 6. When the compressor is operating off design, the losses at the rotor entrance section may be quite large, preventing the design mass flow from passing through the minimum area, or conditions may exist causing flow separation in the rotor passage and thus rendering a portion of the flow passage unavailable. One or both of these factors may prevent the rotor from establishing its design entrance condition. Local flow separation on the suction surface may also prevent the establishment of the design compression-wave system. A study of the losses and the accompanying utilization of the passage minimum flow area will be considered in the following discussion.

Equivalent supersonic cascade operation. - The influence of flow separation was investigated analytically by computing the performance of the cascade. The cascade geometries were equivalent to the rotor pitch sections used in this investigation. No reliable information concerning the extent of the boundary-layer build-up or the possibility of flow separation at the passage minimum-area section is available. As a consequence, the flow area required for a flow Mach number of 1.0 expressed as a fraction of the geometric area was considered a variable and was termed the effective minimum area.

Operation of the cascade at incidence angles other than design would require an extended wave system (bow waves). The total-pressure recovery through the wave system and the required effective minimum area can be approximated for any given incidence angle and entrance Mach number as given in appendix B. The results of this computation for the cascades representing the original and modified compressor rotors are presented in figure 11. Curves of constant Mach number are plotted

over a range of suction-surface incidence angle against effective minimum area. Calculated total-pressure-recovery contours are also shown on this figure.

Operation with the design wave configuration would require an incidence angle of sufficient magnitude to account for the leading-edge thickness (the original cascade would require about 2.0° and the modified cascade would require about 0.1°). A deficiency in minimum area would in general result in an increased incidence flow angle and would be accompanied by a bow wave. The cascade of the original compressor rotor blades operating at a Mach number of 1.65 would require an effective minimum area of 1.0 to achieve a suction-surface incidence angle of 0.9°. The modified cascade, on the other hand, indicates that the design entrance conditions could be achieved at an entrance Mach number of 1.65 with an effective minimum area of 0.98. The reason for this difference is the allowance made for boundary layer in the design of the modified blade section. A deficiency in effective minimum area in the modified cascade results in a smaller incidence angle than with the original cascade for given inlet Mach number. The calculated total-pressure recoveries for the modified cascade result in curves of different slope than for the original cascade; this is a result of the change in magnitude of the losses combined to obtain the calculated total-pressure-recovery variation with incidence. The effect of decreasing the inlet Mach number for a fixed effective area ratio is to increase the required incidence angle for both cases. The original rotor tended to decrease the total-pressure recovery slightly at lower Mach numbers and fixed effective areas, while the modified rotor tended to increase the recovery slightly. In spite of the change in slope of the total-pressure-recovery contours, at a given inlet Mach number and incidence angle, the entrance-region total-pressure recovery is always higher in the original than in the modified cascade.

Relation of constant-speed rotor operation to cascade. - The rotor-inlet relative Mach number for a given incidence angle was computed with the design rotor speed and guide-vane turning. The relation between design-speed rotor and cascade operation is shown in figure 11. The compromise made in the modification can be illustrated by comparing the rotor performance lines. The original rotor would obtain a very high total-pressure recovery (0.975) provided its entrance conditions could be established. Since it was not possible to obtain the small design angle of incidence, the rotor contraction ratio was reduced by the described modification. In so doing, the entrance-section total-pressure recovery would be reduced at the design incidence to about 0.928. However, at increased incidence angles the calculated losses in the inlet section do not increase as rapidly for the modified rotor as the losses computed for the original rotor. With effective minimum areas less than 0.97, the inlet total-pressure recovery is higher for the modified rotor than for the original rotor.

The maximum and minimum weight-flow data points for the two rotor configurations are shown in figure 11. The maximum weight-flow point represents the closest approach to the design entrance flow. The modification to the rotor resulted in a reduction in incidence angle from 6.65° to 3.3°. The effective minimum area for both configurations was low and approximately the same (original 0.89, modified 0.90). These maximum weight-flow points are obtained in the region where the total-pressure recovery for the modified rotor would be higher than that obtained for the original rotor (original 0.86, modified 0.91). This is substantiated by the slightly higher performance level of the modified compressor rotor.

Flow separation effects. - The effective minimum areas obtained in this investigation indicate area deficiencies greater than those expected from normal boundary-layer build-up. It can be assumed that separated flow regions exist near the minimum-area section. With the flow assumed to follow the blade surface near the leading edge, the gradients near the suction surface of the blade were computed and are shown in figure 12. For the original rotor configuration a gradual reduction in Mach number occurs. For the estimated bow-wave position (for the maximum weight-flow operational point at maximum pressure ratio), the indicated suction-surface Mach number is about 1.23. This Mach number is lower than those usually associated with boundary-layer shock separations for turbulent boundary layers. The modified compressor rotor near its operation point results in a higher Mach number at the bow wave, which is above the Mach number associated with boundary-layer separation. This boundary-layer separation associated with the bow wave may be the cause for the low effective area for the modified compressor rotor.

It was indicated that for the original rotor the flow probably did not separate at the bow wave. However, the large amount of external compression in the original compressor rotor resulted in a very rapid change in blade suction-surface direction at the minimum-area position. Thus, the low effective area obtained for the original rotor may be due to flow separation at the minimum-area section because of the rapid change in blade surface direction.

The preceding considerations resulted by assuming that the flow followed the suction surface of the blade near the leading edge. Similar to the effects observed in spike-type diffusers of the double-cone variety (ref. 10), the flow may separate from the suction surface ahead of the compression wave system, thus causing the compression waves to fall ahead of the passage entrance and to result in an increase in incidence angle. The magnitude of this effect can not be determined from these data, although by considering the blade shape the effect may be more pronounced in the original compressor rotor.

Estimated Performance of Subsonic Portion of Rotor Passage

The measured over-all recovery at the pitch section is tabulated in figure 11. Since this figure indicates the computed recovery over the rotor inlet section, it is possible to estimate the recoveries in the subsonic diffuser section. A comparison will be made at the audible stall point for each rotor. The original rotor obtained a measured over-all recovery of 0.81 at this point, at an incidence angle of about 8.2°, for which the computed inlet-section recovery was about 0.835. Thus, the subsonic diffuser section of the rotor must be operating with a total-pressure recovery of 0.97. These values are to be compared with the modified rotor where a measured over-all recovery of 0.82 was obtained at an incidence angle of about 4.5°. The computed inlet-section total-pressure recovery was about 0.89 and the recovery in the diffusion section was about 0.92. Thus, at the peak total-pressure-ratio point, modification to the rotor has resulted in a decrease in the performance of the subsonic diffuser section of the rotor passage. This result might be expected since, as indicated in the previous discussion, the boundary-layer build-up or flow separation was increased by the modification to the rotor. At the point where each rotor approaches nearest the design point (points A and B, fig. 7), a similar computation indicates that the subsonic section recovery was about 0.90 and 0.87 for the original and modified configurations, respectively.

CONCLUDING REMARKS

The analysis of this investigation indicated that neither the original nor the modified compressor rotor utilized the minimum-area portion of the rotor passage effectively. In the case of the original rotor this may be the effect of the rapid change in direction of the blade suction surface at the minimum section. The modification to the rotor considerably reduced the change in direction required at the minimum section; however, it resulted in an increase in the Mach number at which the normal shock encountered the suction-surface boundary layer. Apparently both conditions resulted in extensive flow separation, with the original configuration utilizing the minimum area slightly more effectively. Thus, this type of modification to improve the entrance conditions has not resulted in an appreciable improvement in performance. It might be expected that the best compromise between these conflicting conditions would result in only a small improvement in rotor performance.

The data have indicated that, as applied to the rotors of this investigation, the principle of external compression could probably not be improved to any large extent by blade modifications of the type used. If the flow separation is assumed to take place mainly on the blade suction surface, the desirability of reducing the number of blades might be considered. For example, the best improvement that might be considered by reducing the number of blades by half would be that the deficiency

in minimum area might be decreased by half. This would be accompanied by an increase in inlet-section total-pressure recovery. Of course, the three-dimensional effects were not considered in this case and the blade chord would of necessity be longer.

The preceding discussion has indicated the difficult problem of improving the performance of the external-compression-type compressor rotor. (On a two-dimensional basis, a basic difficulty exists in the idea of external compression in that the compression of the stream in the passage entrance region must be accomplished by turning the flow in the direction opposite to rotor rotation. This is opposite to the direction of adding energy to the fluid and results in the large change in direction of the blade suction surface at the minimum passage section.) The effect of external compression is to decrease the streamline area in the blade inlet region by a series of compression waves, thus effecting a reduction in flow Mach number at the passage-inlet closure line. The same effect on Mach number could be obtained by a radial reduction in streamline area; this would apparently achieve the desired results without turning the flow counter to the direction of rotation and without the accompanying undesirable features. Although no quantitative statements can be made, it appears that this external-compression design on a three-dimensional basis may be more desirable than the two-dimensional design considered in this investigation.

SUMMARY OF RESULTS

The results of this investigation of two configurations of external compression applied to a 16-inch supersonic-compressor rotor can be summarized as follows:

1. With design external compression to a Mach number of 1.0, the compressor rotor was not able to achieve the design entrance conditions. The reason for this angle of incidence of 6.6° to 8.2° at the rotor pitch section at design speed could not be ascertained from the experimental data.

2. The modification to the rotor blades which reduced the external compression and decreased the design contraction ratio was made to compromise the design performance in order to improve the entrance conditions. This resulted in an increase in peak total-pressure ratio from 2.20 to 2.27 and a corresponding increase in adiabatic efficiency from 0.72 to 0.76, accompanied by an increase in equivalent weight flow from 21.4 to 23.2 pounds per second and a decrease in deviation from design inlet relative angle from 6.6° to 3.3°. The modified external-compression rotor more nearly achieved the design inlet relative flow angle.

3. The analysis indicated that neither the original nor the modified rotor utilized the minimum-area section effectively, indicating the presence of extensive boundary-layer build-up or flow separation.

4. The investigation indicated that this type of modification might be expected to result in only a limited improvement in performance. This type of modification increases the Mach number at which a normal-shock - boundary-layer interaction occurs and thus reduces the advantage of external compression.

5. The analysis indicates that at least part of the reason for failure to establish the entrance conditions is probably the lack of knowledge of the losses accompanying the boundary-layer build-up and flow separation in the entrance and minimum-area sections of the compressor rotor passage during off-design operation.

Lewis Flight Propulsion Laboratory
National Advisory Committee for Aeronautics
Cleveland, Ohio, July 27, 1954

APPENDIX A

SYMBOLS

The following symbols are used in this report:

A	area, sq ft
A_{cr}/A	critical area ratio
C	contraction ratio, inlet area/throat area, (design)
c	distance from blade leading edge along chord, in.
h	distance from blade chord to upper surface, in.
i	incidence angle, deg
l	distance from blade chord to lower surface, in.
M	Mach number
M'	Mach number relative to rotor
M_u	rotor speed on basis of Mach number
n	number of rotor blades
P	total pressure, in. Hg
P'	total pressure relative to rotor
p	static pressure
r	radius, ft
s	portion of passage spilled (stagnation streamline displacement for an infinite cascade), $Y_s/(2\pi r/n)\cos \beta_e$
t	blade thickness, in.
U	rotor speed, ft/sec
v	flow velocity, ft/sec
$W\sqrt{\theta}/\delta$	weight flow at standard sea-level entrance conditions, lb/sec
x	distance along abscissa in coordinate axis of cascade

Y_s displacement of stagnation streamline from blade tip

y distance along ordinate in coordinate axis of cascade

β angle of air flow measured by instruments from rig axis, deg

β' angle of air flow relative to blade measured from rig axis, deg

δ angle of blade suction surface from coordinate axis in cascade, deg

ϵ blade leading-edge wedge angle, deg

η_{ad} adiabatic efficiency

Θ angle of infinitesimal Mach wave measured from coordinate axis of cascade, deg

θ compression wave angle, deg

ν Prandtl-Meyer angle, deg

ρ density, lb/cu ft

φ maximum change in blade angle at ramp section, deg

Subscripts:

a conditions ahead of cascade blade

b effective conditions immediately behind bow wave

c conditions at blade minimum section

e conditions between blade leading edge and blade ramp of cascade

i incidence

n point along blade ramp of cascade

u tangential component of rotor

z axial component

0 upstream stagnation condition in depression tank

1 instrument survey station 1 between guide vanes and rotor (fig. 5)

[redacted]

2 instrument survey station 2 immediately behind rotor (fig. 5)

3 instrument survey station 3 downstream of rotor (fig. 5)

APPENDIX B

COMPUTATION OF APPROXIMATE LOSSES AT ROTOR ENTRANCE SECTION

Considerable difficulty has been encountered in establishing the desired entrance conditions to the external-compression supersonic-compressor rotors. Reference 6 dealt with these problems and indicated that theoretically, for the supersonic cascade being considered, the desired entrance conditions could be established. Methods similar to those of the reference will be applied to the original and modified compressor rotors used in this investigation.

A cascade of blades operating at supersonic velocities and without back pressure or choking fixes the upstream flow direction parallel to the blade suction surface at the closure line. The closure line may be defined as the Mach line generated on the suction surface and intersecting the leading edge of the adjacent blade. (This condition has been discussed in refs. 11 and 12). Lowering the back pressure or raising it slightly as long as it does not affect the closure line will not alter the upstream conditions. If the back pressure is increased until it affects the flow (by diffusion to subsonic velocities or over the entire region) at or ahead of the closure line, the inlet flow configuration will be changed. The result will be an increased flow angle into the cascade. In order that the flow may enter at this increased angle, expansion waves must pass upstream of the cascade and they must be accompanied by a bow wave to support them in the steady state (see fig. 13). This off-design entrance configuration, supported by the application of back pressure on the cascade, determines the magnitude of the losses encountered. In view of these losses, the minimum flow area may not be sufficient to pass the mass flow. In this case the strength of the bow wave must be increased to support further adjustment of the upstream flow. On the other hand, if the losses are such that the minimum-area section can pass the mass flow at a Mach number of 1.0 or less, the off-design configuration described can exist as a somewhat stable operating condition. In the case of the compressor rotor, it must be possible to obtain the design entrance conditions by reducing the back pressure. This can be done only as long as the Mach number at the minimum section is less than 1.0. To determine the off-design characteristics and the flow conditions at the minimum-area section, a knowledge of the entrance-section total-pressure recovery is necessary. In the following discussion, these losses are approximated.

Methods

The assumed flow configurations for this off-design operation of a cascade of blades is shown in figure 13. In this case the flow is assumed restricted by the throat area, which caused the bow wave at the passage entrance (designated d-f in fig. 13). After passing through the

bow wave, the flow is turned to the suction surface of the blade by a series of expansion waves (originating at a). The flow between the blade suction surface and the stagnation streamline must pass through a series of compression waves (region b-d-e) and a normal shock near the passage entrance (e-d). The normal shock is considered as an extension of the bow wave to the blade suction surface. The bow wave (d-f) and the normal shock extension (e-d) are the two sources of loss that are to be considered. The losses in the bow wave have been investigated in references 12 and 13. Sufficient equations are available to determine by a reiteration process values for the angle of incidence, the displacement of the stagnation streamline (or spillage), total-pressure recovery, and the effective Mach number behind the bow wave at a given upstream Mach number. To determine the total-pressure recovery over the normal shock, it is necessary to determine the variation of Mach number ahead of the normal shock. After the variation in Mach number is determined, increment losses are summed over the passage entrance. The total-pressure recoveries in the bow wave and the normal-shock extension are combined such that the normal shock and the bow wave are spaced the same distance from the blade leading edge. The following discussion deals with the details and results of this computation.

Bow-Wave Total-Pressure Recoveries

The total-pressure recovery of the assumed bow wave is related to the magnitude of the spillage s and to the upstream flow direction by the following two equations derived from the requirement for continuity:

$$\left(\frac{A_{cr}}{A}\right)_a \frac{\cos \beta_a}{\cos \beta_e} = \left(\frac{A_{cr}}{A}\right)_e \left(1 - \frac{Y_s}{\frac{2\pi r}{n} \cos \beta_e}\right) \frac{P_b}{P_a} \tag{B1}$$

(eq. (B2), ref. 6). Equation (B1) can be solved for $\frac{Y_s}{\frac{2\pi r}{n} \cos \beta_e}$, which was defined as the spillage s, since $(A_{cr}/A)_a$, $\cos \beta_a$, and $\cos \beta_e$ are known from the geometry and the set upstream conditions, $(A_{cr}/A)_e$ can be computed from the required expansion from β_a to β_e, and P_b/P_a is initially assumed equal to 1.0. The total-pressure loss P_b/P_a across the bow-wave configuration is determined from the spillage and Mach number M_a according to the equation (eq. (3), ref. 12):

$$\left(1 - \frac{P_b}{P_a}\right) = s \int_0^{\infty} \left(1 - \frac{P_y}{P_a}\right) d\left(\frac{y}{Y_s}\right) \tag{B2}$$

[redacted]

The term $\int_0^\infty \left(1 - \frac{P_y}{P_a}\right) d\left(\frac{y}{Y_s}\right)$ is a function of the Mach number M_a only ($M_a = M_1$ of ref. 12) and has been evaluated over the desired range of Mach number (ref. 12). Since s was calculated from equation (B1), P_b/P_a can be obtained from equation (B2). The computation procedure can then be repreated using the recovery for the bow wave. The effect of the recovery through the bow wave is considered by assuming that the effective Mach number behind the bow wave can be obtained from the ratio $(A_{cr}/A)_b$ as given in the following equation:

$$\left(\frac{A_{cr}}{A}\right)_b = \left(\frac{A_{cr}}{A}\right)_a \frac{P_b}{P_a} \tag{B3}$$

The b conditions are considered as the effective conditions behind the bow wave, and isentropic expansion from β_b to β_e is used to determine the flow conditions at e.

This computational procedure may be repeated until the value of spillage, total-pressure recovery, and Mach number on the suction surface are all satisfied in the equation used. This computation was carried out for a range of suction-surface incidence angle and Mach number.

An example of these computations is shown in figure 14 where the total-pressure recovery, spillage, and suction-surface Mach number are plotted against suction-surface incidence angle i ($i = \beta_a - \beta_e$) for an inlet Mach number of 1.5 and a design entrance flow angle of $\beta_e = 63.35^\circ$. The total-pressure recovery is 1.00 at the design flow angle ($i = 0$) and falls off very rapidly as the suction-surface incidence angle increases (being about 0.923 at $i = 6.0^\circ$). The spillage s varies from 0 to 0.125 over the previously considered range ($i = 0^\circ$ to 6.0°). The Mach number on the suction surface of the blade increases from 1.5 to about 1.552 at an incidence angle of about 4.65°. At this point, however, the losses in the bow wave become large enough to offset the effect of the expansion, and the suction-surface Mach number no longer increases. This point may represent the limit of reliability of the assumptions made in this computation.

Total-Pressure Recovery Over Normal Shock Near Passage Entrance

Besides the total-pressure recovery in the bow wave, the losses in the assumed normal shock near the passage entrance section must be determined. This normal shock will be considered as an extension of the bow wave as indicated in figure 13. With the type of blade (compression ahead of the passage closure) used in this investigation, the Mach

number along this normal shock wave varies from the suction-surface Mach number M_a to some rather low value. To approximate the losses over this normal shock, the distribution of Mach number in this region will be determined.

To map the Mach number distribution in the entrance region, a coordinate system was established with the x-axis coincident with the suction surface of the blades. From the blade coordinates a curve of blade thickness could then be plotted above the coordinate axis t and the slope of the suction surface δ relative to the coordinate axis. Increments of the blade surface slope were then selected (1.0° in this case) at which the compression wave angle θ could be determined for the Mach number at the given point. The Mach number can be determined and is constant along this wave front, which has an absolute slope $\Theta_n = (\theta_n + \delta_{n-1})$ at the given intervals. The equation for these compression waves then can be expressed as

$$(y - t_n)/(x - x_n) = \tan \Theta_n \qquad (B4)$$

This equation can then be solved for x at the desired values of y. This process was carried out for increments of blade slope δ and for y, and the Mach number distribution with a suction-surface Mach number M_e of 1.5 is shown for the original rotor blades used in this investigation in figure 15. The change in Mach number near the compression ramp ($y = 0.1$ in.) is very gradual from the upstream Mach number M_e to the Mach number after the compression ramp (in this case, M_c is decreased to near 1.0). However, the change in Mach number is very rapid near the next blade (i.e., $y = 0.6$ in.). The fact that these curves become vertical indicates coalescence of the waves and a resultant strong shock.

The total-pressure recovery over this assumed normal shock can then be determined at any desired value of x by summing the incremental total-pressure recoveries. It was noted above that the Mach number curves became vertical at some points and that this indicates coalescence. For these conditions the normal-shock recovery was obtained for the increased Mach number at the point at which coalescence was obtained.

The total-pressure recovery is plotted against distance for several values of spillage for the original rotor in figure 16. For zero spillage the total-pressure recovery over this region varies from 0.9915 at $x = 1.35$ inches to about 0.9575 at $x = 1.0$ inch. As the percent spillage s is increased, the recovery over this region is increased as a result of removing a portion of the field over which low recovery is obtained.

Total-Pressure Recovery of Entrance Section and Flow Conditions at Minimum-Area Section

Two contributing factors to the total-pressure recovery (bow-wave recovery and the extending normal shock near the passage entrance) have been considered separately and were computed over the desirable range of conditions. It was necessary to combine these two solutions at the proper conditions to determine the cascade performance. The assumptions pertaining to the bow wave relate the spillage value to the distance the bow wave may extend ahead of the rotor blades and are given on figure 3 of reference 13. It was assumed that the bow-wave solution then located the normal shock and that the coalescence was not appreciably affecting the location of the shock system. Thus, by picking an inlet flow condition and determining the loss in the normal shock near the entrance section for the Mach number on the suction surface of the blade and the shock location indicated, the total-pressure recovery over the normal shock was computed and combined with the bow-wave total-pressure recovery to obtain the total-pressure recovery over the entrance region of the cascade. With this total-pressure recovery, the flow conditions at the minimum-area section of the rotor can be determined by the following equation (eq. (B3) of ref. 6):

$$\left(\frac{A_{cr}}{A}\right)_a \frac{\cos \beta_a}{\cos \beta_e} = \left(\frac{A_{cr}}{A}\right)_c \frac{P_c/P_a}{C} \qquad (B6)$$

From this equation, $(A_{cr}/A)_c$ can be determined. If the calculated value of $(A_{cr}/A)_c$ is greater than 1.0, the losses are such that the flow cannot pass through the minimum section, and, consequently, the assumed upstream conditions could not be established. On the other hand, if $(A_{cr}/A)_c$ is less than 1.0, two interpretations are possible: (1) it can be assumed that the total minimum area is effective, and thus $(A_{cr}/A)_c$ can be used to determine the minimum section Mach number. (2) It might be assumed that the minimum-area section is not being utilized completely because of boundary-layer build-up or flow separation and that the flow Mach number at the minimum section is very nearly 1.0. Then the term $(A_{cr}/A)_c$ can be considered as the fraction of the minimum area that is effective. True conditions undoubtedly lie somewhere between these two cases, but for the purpose of this analysis the latter case seems to be the better assumption.

[redacted]

REFERENCES

1. Kantrowitz, Arthur: The Supersonic Axial-Flow Compressor. NACA Rep. 974, 1950. (Supersedes NACA ACR L6D02).

2. Erwin, John R., Wright, Linwood C., and Kantrowitz, Arthur: Investigation of an Experimental Supersonic Axial-Flow Compressor. NACA RM L6J01b, 1946.

3. Johnsen, Irving A., Wright, Linwood C., and Hartmann, Melvin J.: Performance of 24-Inch Supersonic Axial-Flow Compressor in Air. II - Performance of Compressor Rotor at Equivalent Tip Speeds from 800 to 1765 Feet per Second. NACA RM E8G01, 1949.

4. Lown, Harold, and Hartmann, Melvin J.: Investigation of a 24-Inch Shock-in-Rotor Type Supersonic Compressor Designed for Simple Radial Equilibrium Behind Normal Shock. NACA RM E51H08, 1951.

5. Nussdorfer, T. J.: Some Observations of Shock-Induced Turbulent Separation on Supersonic Diffusers. NACA RM E51L26, 1954.

6. Creagh, John W. R., and Klapproth, John F.: Utilization of External-Compression Diffusion Principle in Design of Shock-in-Rotor Supersonic Compressor Blading. NACA RM E53F18, 1953.

7. Tysl, Edward R., Klapproth, John F., and Hartmann, Melvin J.: Investigation of a Supersonic-Compressor Rotor with Turning to Axial Direction. I - Rotor Design and Performance. NACA RM E53F23, 1953.

8. Lieblein, Seymour, Lewis, George W., Jr., and Sandercock, Donald M.: Experimental Investigation of an Axial-Flow Compressor Inlet Stage Operating at Transonic Relative Inlet Mach Numbers. I - Over-All Performance of Stage with Transonic Rotor and Subsonic Stators up to Rotor Relative Inlet Mach Number of 1.1. NACA RM E52A24, 1952.

9. Goldberg, Theodore J., Boxer, Emanuel, and Bernot, Peter T.: Experimental Investigation of an Axial-Flow Supersonic Compressor Having Rounded Leading-Edge Blades with an 8-Percent Mean Thickness-Chord Ratio. NACA RM L53G16, 1953.

10. Moeckel, W. E., Connors, J. F., and Schroeder, A. H.: Investigation of Shock Diffusers at Mach Number 1.85. II - Projecting Double-Shock Cones. NACA RM E6L13, 1947.

11. Wright, Linwood C.: Investigation to Determine Contraction Ratio for Supersonic-Compressor Rotor. NACA RM E7L23, 1948.

12. Graham, Robert C., Klapproth, John F., and Barina, Frank J.: Investigation of Off-Design Performance of Shock-in-Rotor Type Supersonic Blading. NACA RM E51C22, 1951.

13. Moeckel, W. E.: Approximate Method for Predicting Form and Location of Detached Shock Waves Ahead of Plane or Axially Symmetric Bodies. NACA TN 1921, 1949.

[redacted]

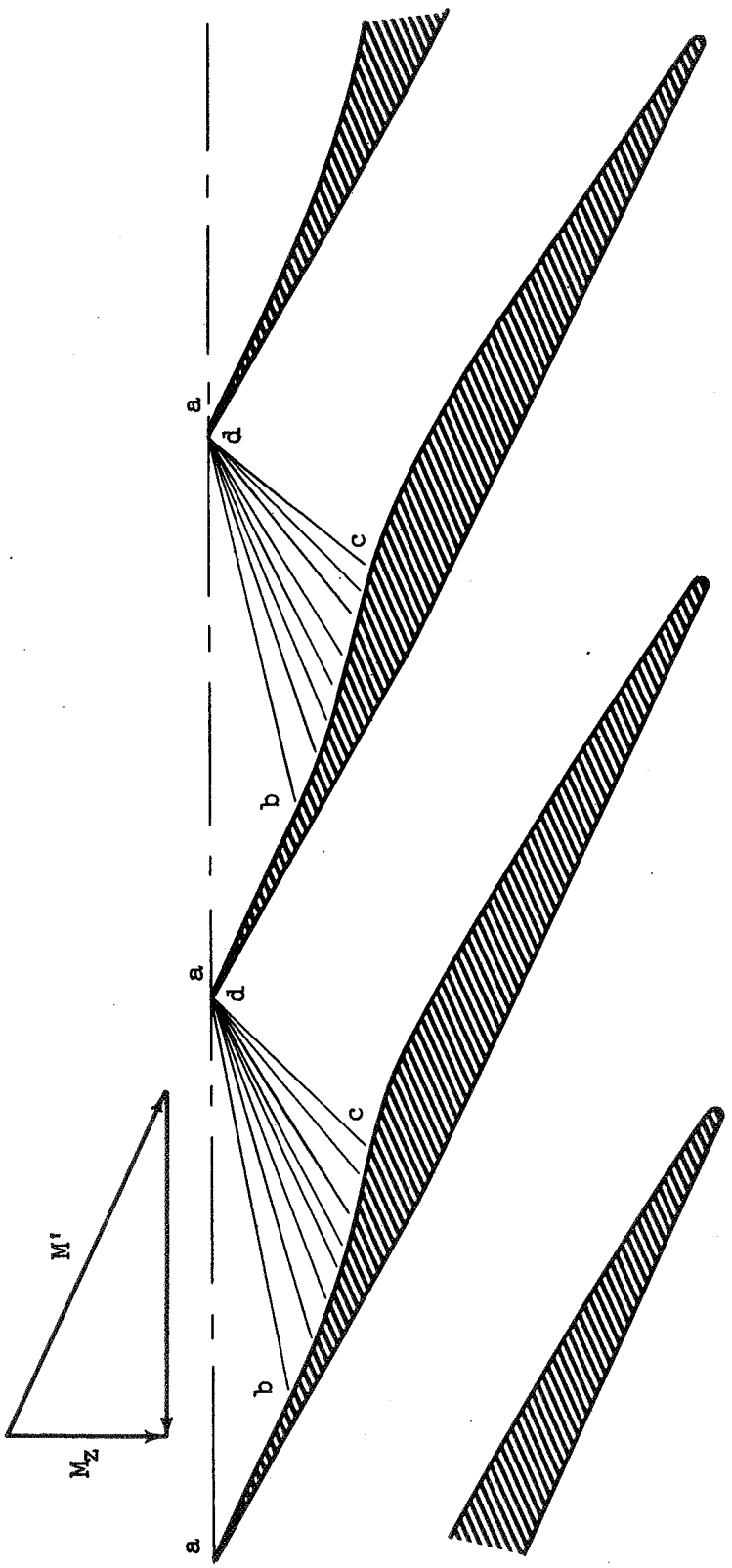

Figure 1. - Application of spiked-diffuser principle to cascade of blades.

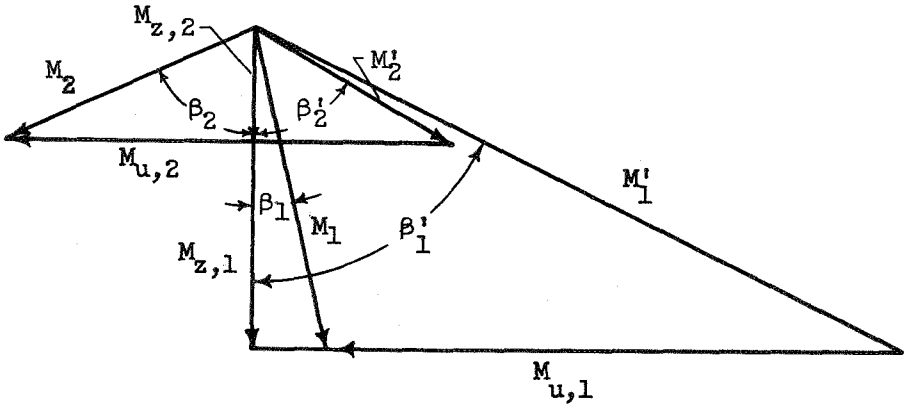

	Original			Modified		
	Tip	Pitch	Root	Tip	Pitch	Root
M_1	0.732	0.737	0.752	0.661	0.656	0.680
$M_{z,1}$	0.730	0.719	0.676	0.659	0.646	0.621
U	1600 ft/sec	1400 ft/sec	1200 ft/sec	1600 ft/sec	1400 ft/sec	1200 ft/sec
M_1'	1.71	1.64	1.61	1.67	1.56	1.52
β_1	$3^\circ0'$	$12^\circ30'$	$26^\circ0'$	$3^\circ0'$	$10^\circ11'$	$24^\circ0'$
β_1'	$64^\circ42'$	$64^\circ0'$	$65^\circ9'$	$66^\circ27'$	$65^\circ33'$	$65^\circ57'$
M_2	0.830	0.693	0.597	0.827	0.691	0.582
M_2'	0.497	0.522	0.472	0.500	0.539	0.505
$M_{z,2}$	0.242	0.264	0.252	0.243	0.272	0.269
β_2	$73^\circ3'$	$67^\circ38'$	$65^\circ2'$	$72^\circ52'$	$66^\circ46'$	$62^\circ28'$
β_2'	$60^\circ54'$	$59^\circ41'$	$57^\circ46'$	$60^\circ54'$	$59^\circ41'$	$57^\circ46'$

Figure 2. - Design velocity diagrams for 16-inch external-compression compressor rotor.

[redacted]

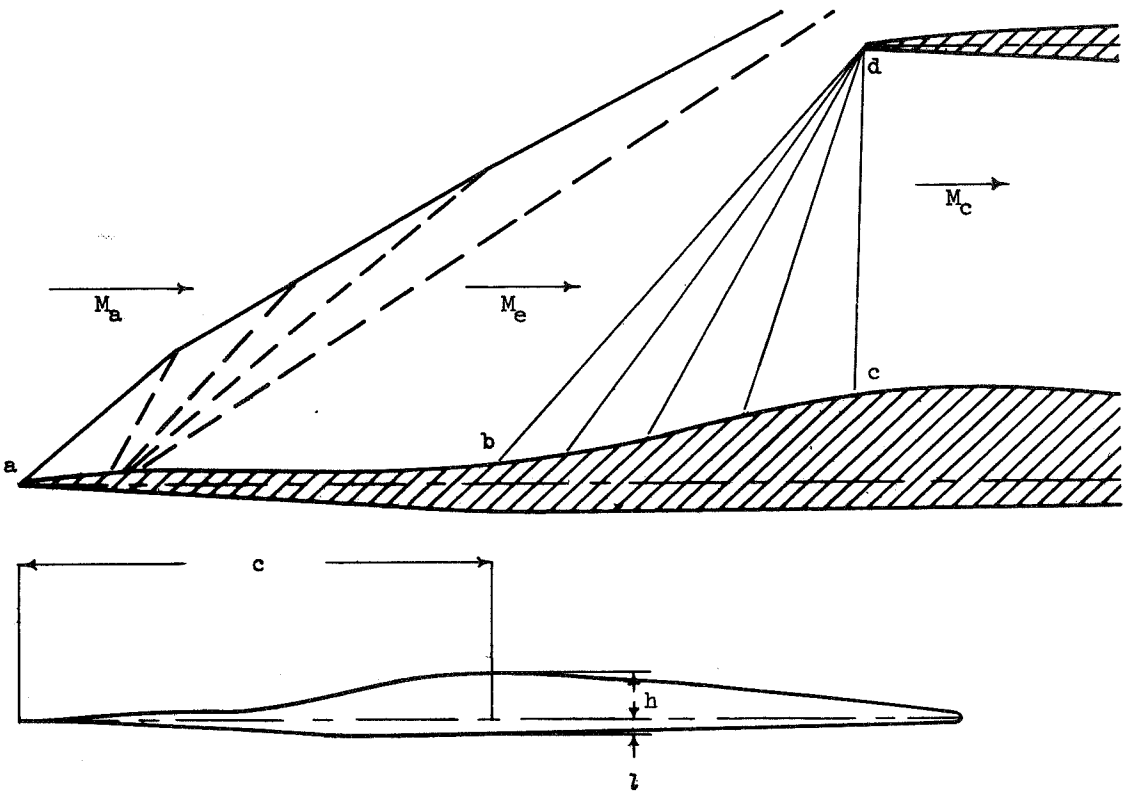

c	h	c	l
0.000	0.004	0.000	0.002
.243	.022	.500	.029
.500	.025	.900	.042
.600	.028	1.000	.045
.700	.033	1.200	.045
.800	.042	1.800	.038
.900	.055	2.987	.0125
1.000	.072	3.000	.000
1.100	.093		
1.200	.117		
1.300	.139		
1.400	.150		
1.500	.152		
1.636	.147		
1.800	.137		
2.100	.115		
2.500	.073		
2.987	.0125		
3.000	.000		

(a) Original configuration.

Figure 3. - Sketch of design flow configuration and blade coordinates for 16-inch external-compression supersonic-compressor rotor at pitch section.

[redacted]

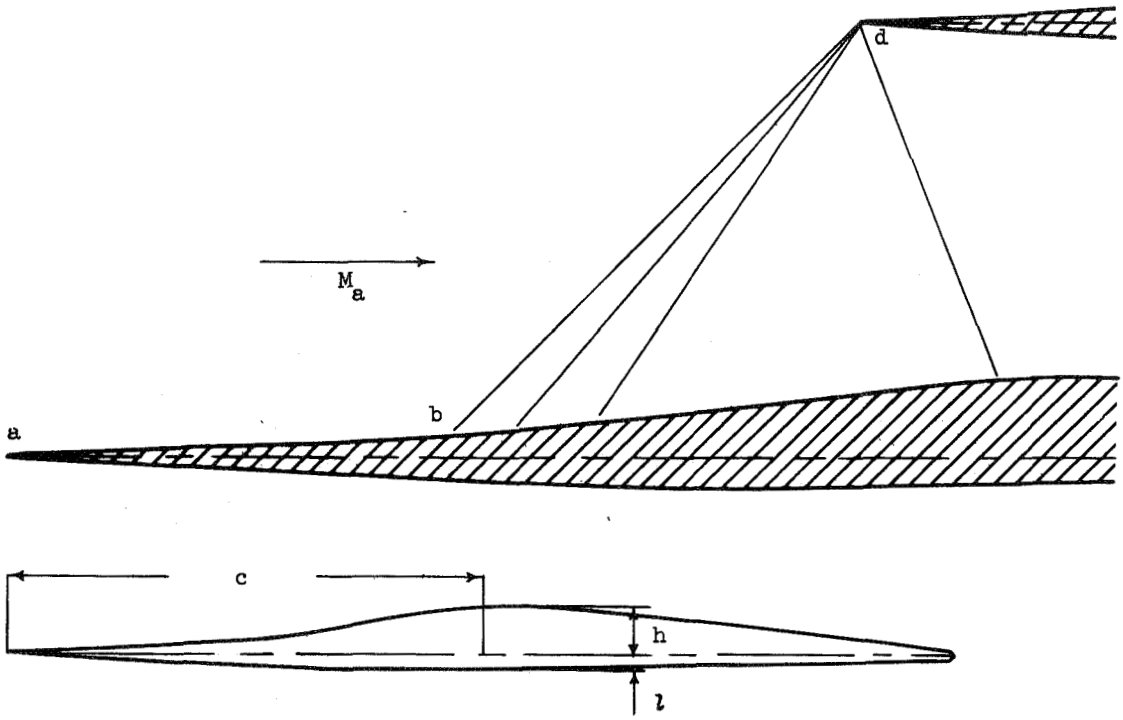

c	h	c	l
0.000	0.004	0.000	0.002
.300	.016	.500	.029
.600	.028	.900	.042
.700	.033	1.000	.045
.800	.042	1.200	.045
1.100	.075	1.800	.038
1.400	.109	2.987	.0125
1.500	.121	3.000	.000
1.600	.128		
1.660	.131		
1.720	.130		
1.900	.118		
2.100	.105		
2.300	.093		
2.500	.073		
2.9875	.0125		
3.000	.000		

(b) Modified configuration.

Figure 3. - Concluded. Sketch of design flow configuration and blade coordinates for 16-inch external-compression supersonic-compressor rotor at pitch section.

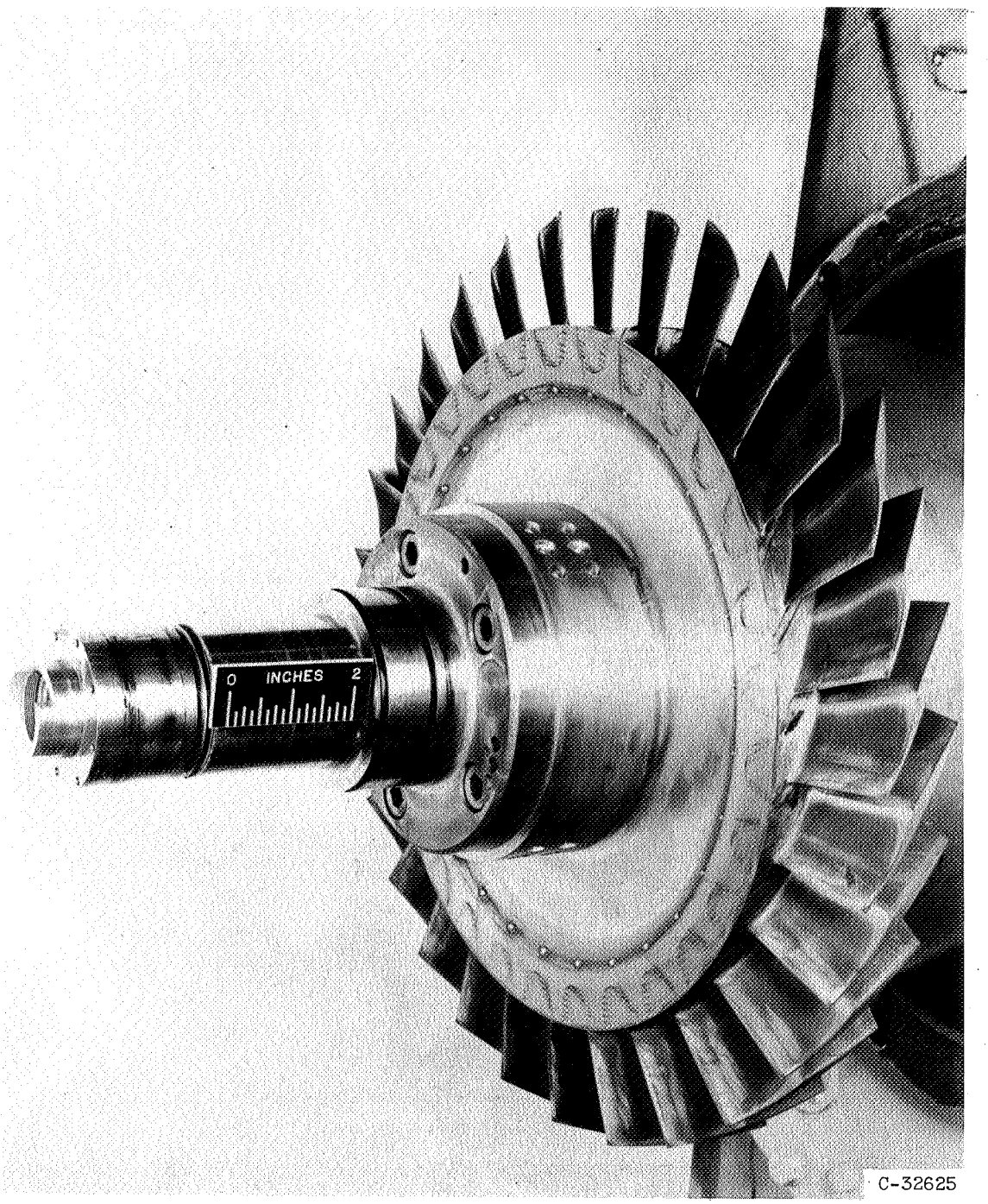

Figure 4. - 16-Inch supersonic-compressor rotor with external compression.

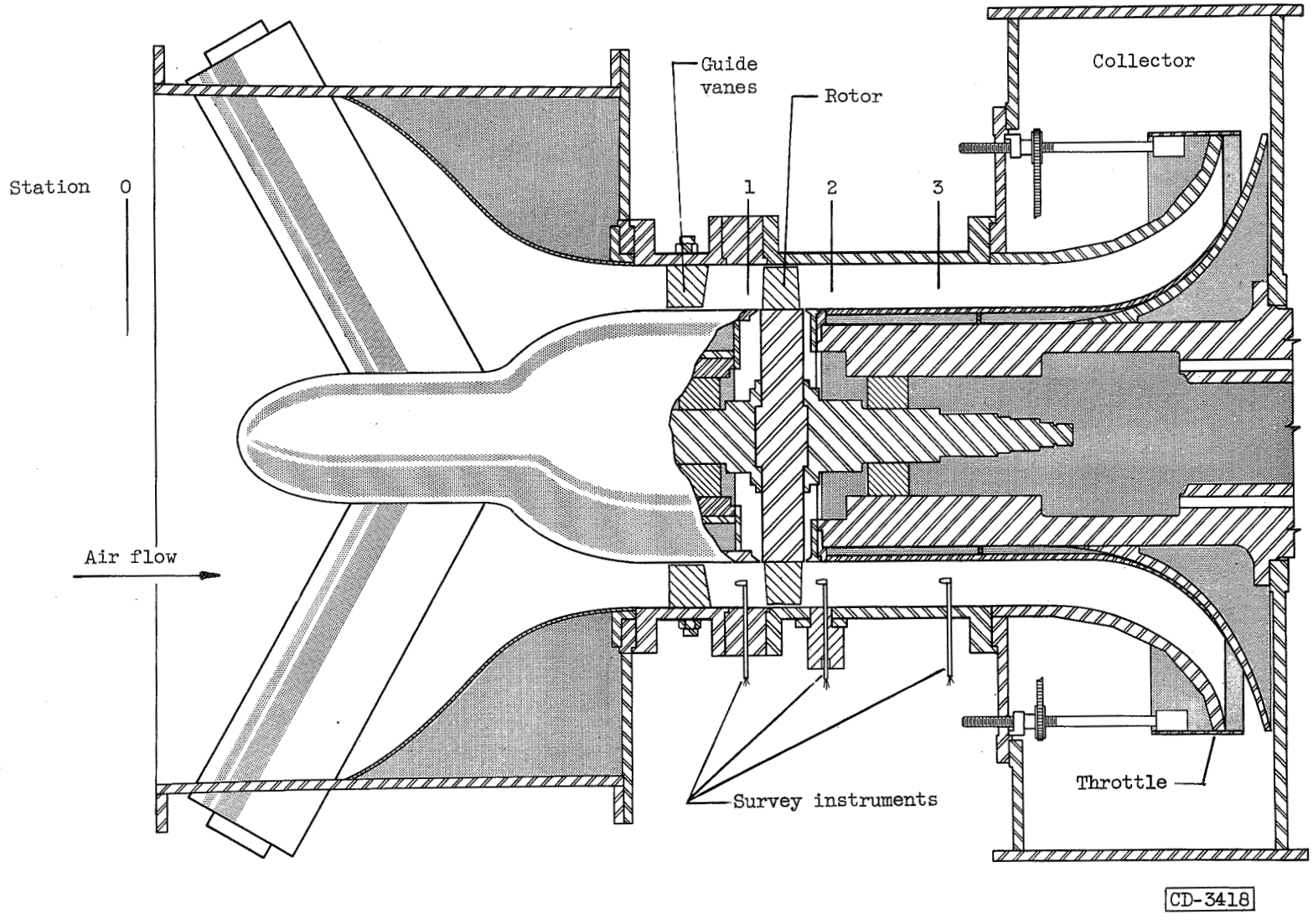

Figure 5. - Schematic diagram of 16-inch supersonic compressor rotor with external compression installed in variable-component test rig, showing instrument stations and guide vanes.

Figure 6. - Pressure and temperature instruments.

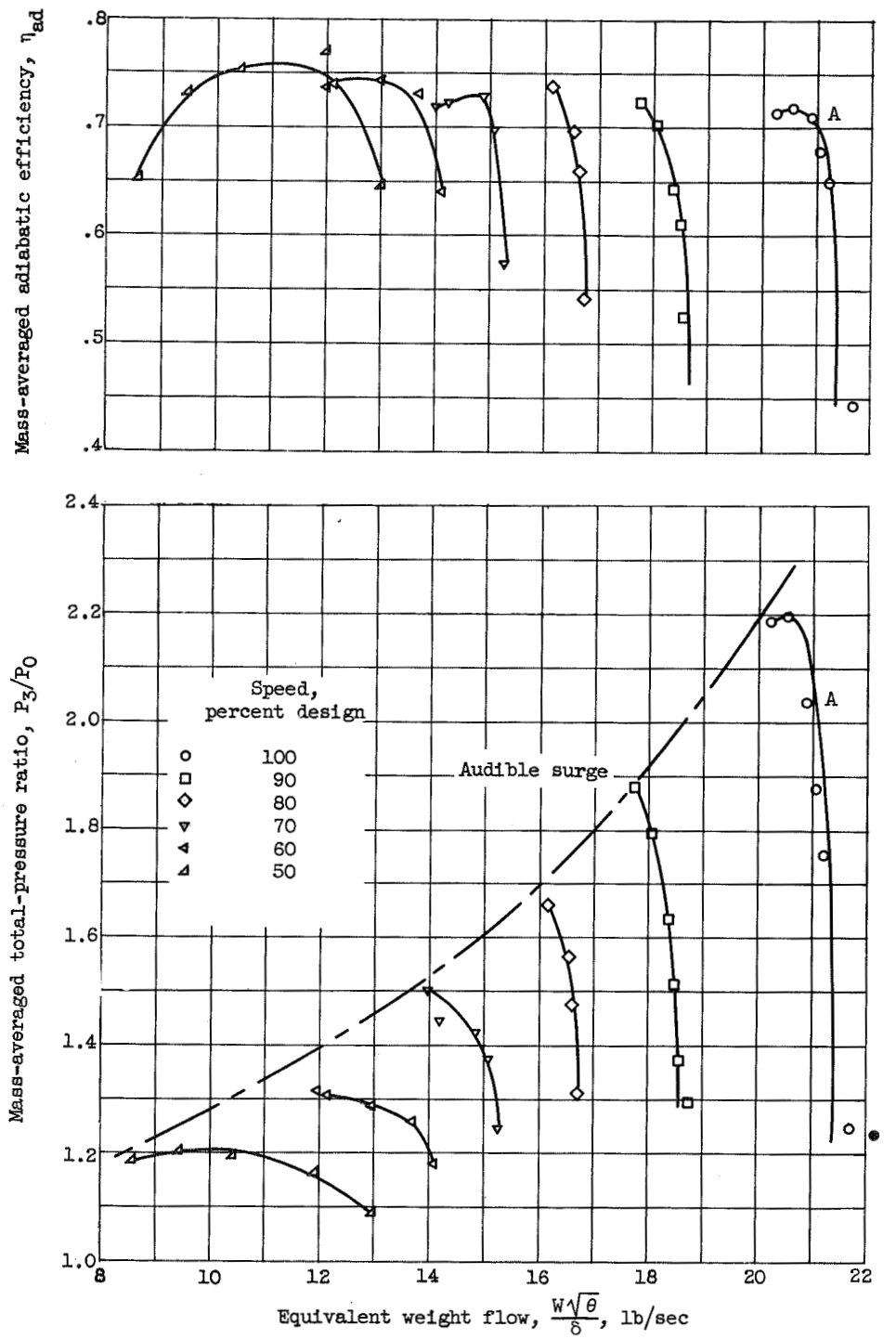

(a) Original configuration.

Figure 7. - Performance characteristics of 16-inch shock-in-rotor type supersonic-compressor rotor component with external compression.

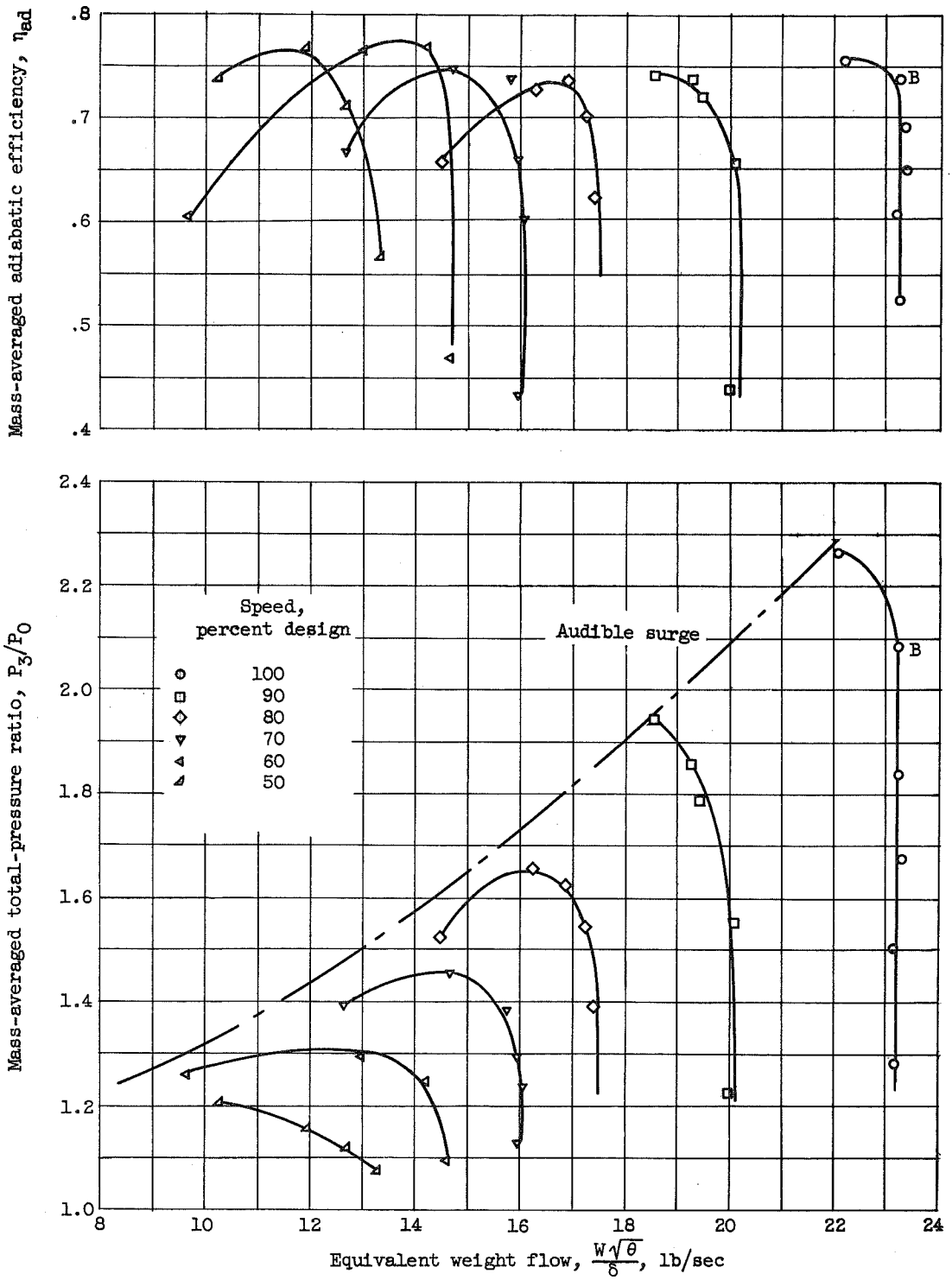

(b) Modified entrance section.

Figure 7. - Concluded. Performance characteristics of 16-inch shock-in-rotor type supersonic-compressor rotor component with external compression.

[redacted]

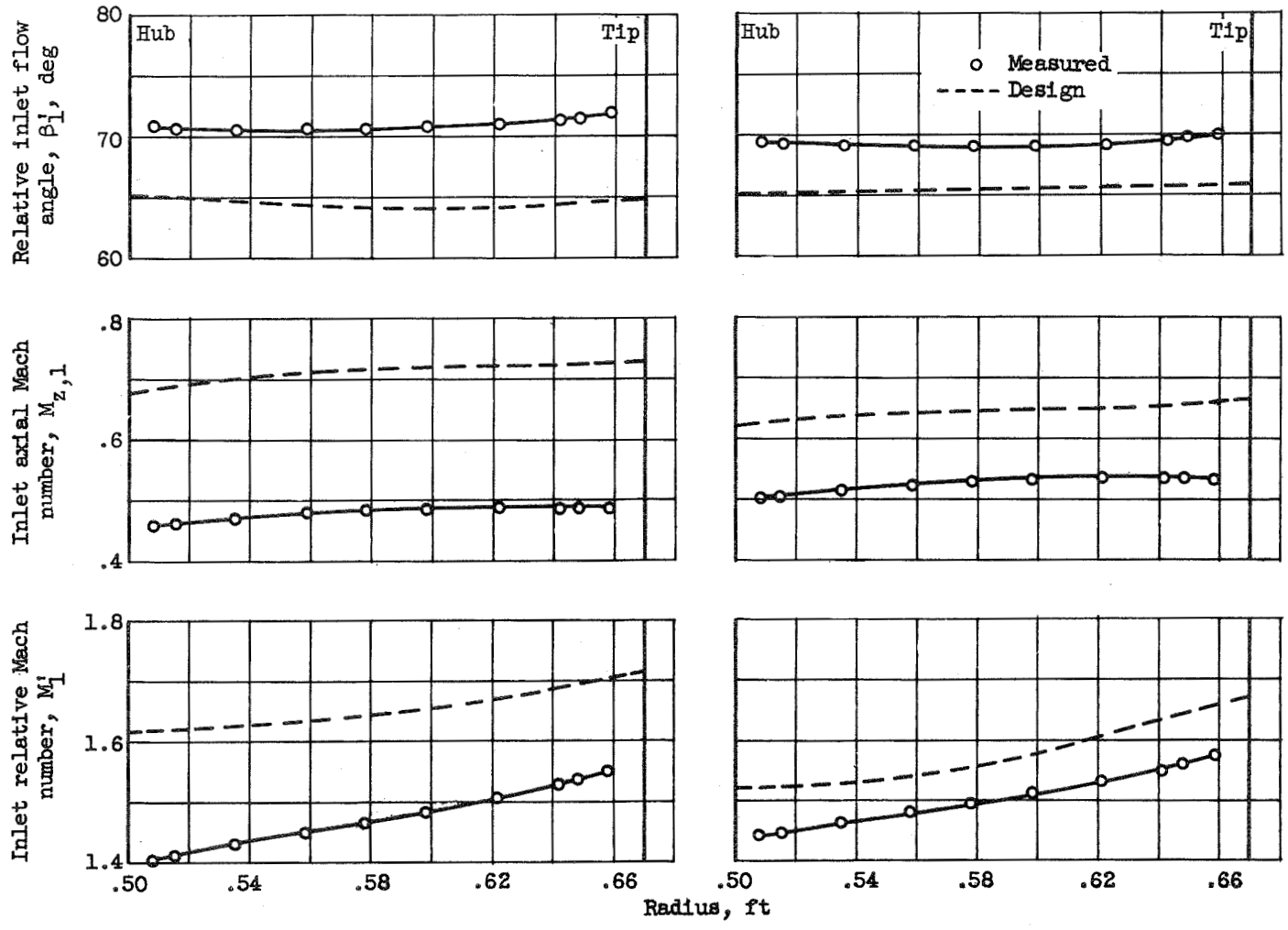

(a) Original rotor.

(b) Modified rotor.

Figure 8. - Inlet conditions for original and modified external-compression rotors at design speed and maximum pressure ratio at maximum weight flow (points A and B of fig. 7).

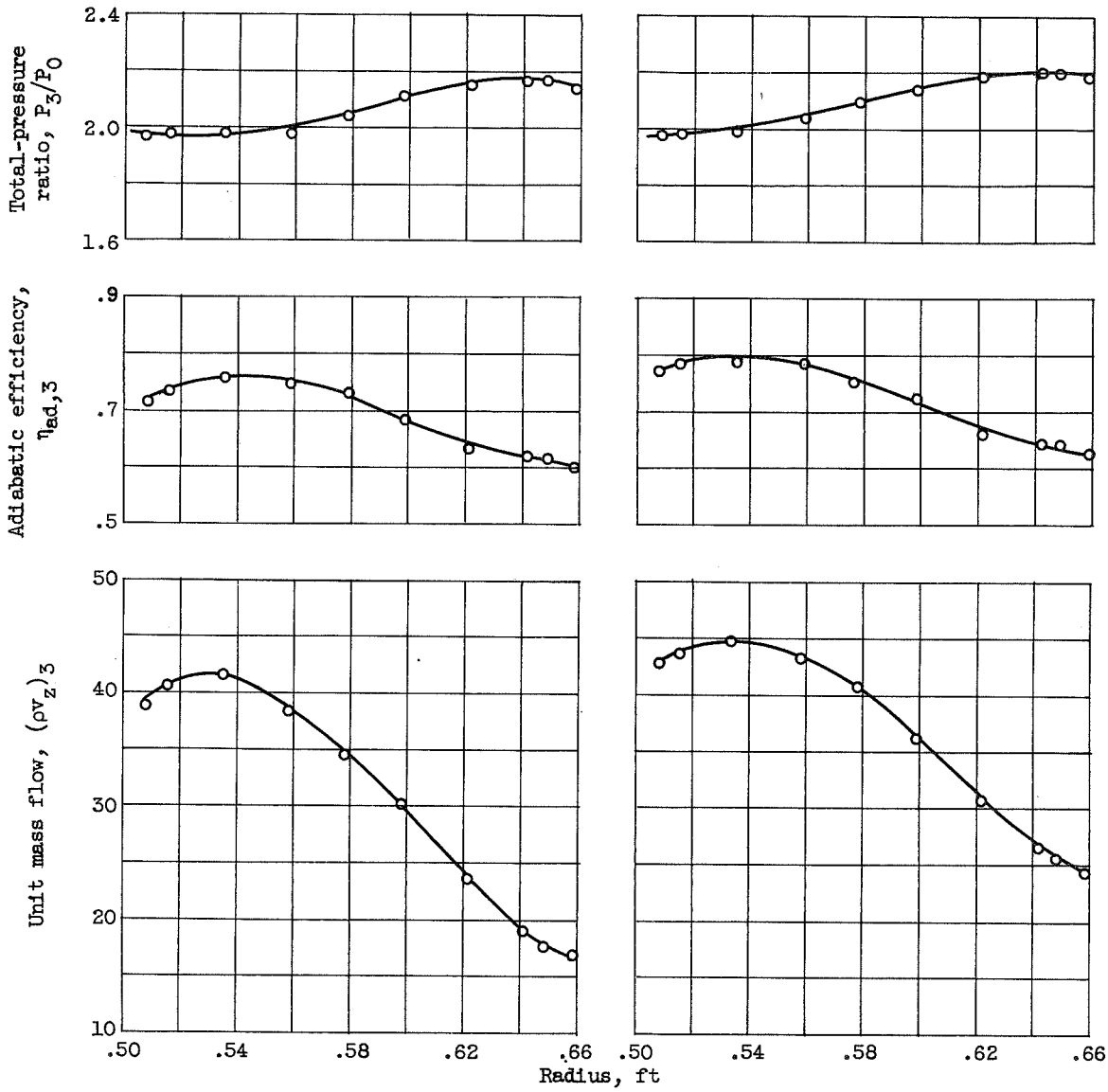

(a) Original rotor. (b) Modified rotor

Figure 9. - Performance of 16-inch external-compression rotor at design speed and maximum pressure ratio at maximum weight flow (points A and B of fig. 7).

[redacted]

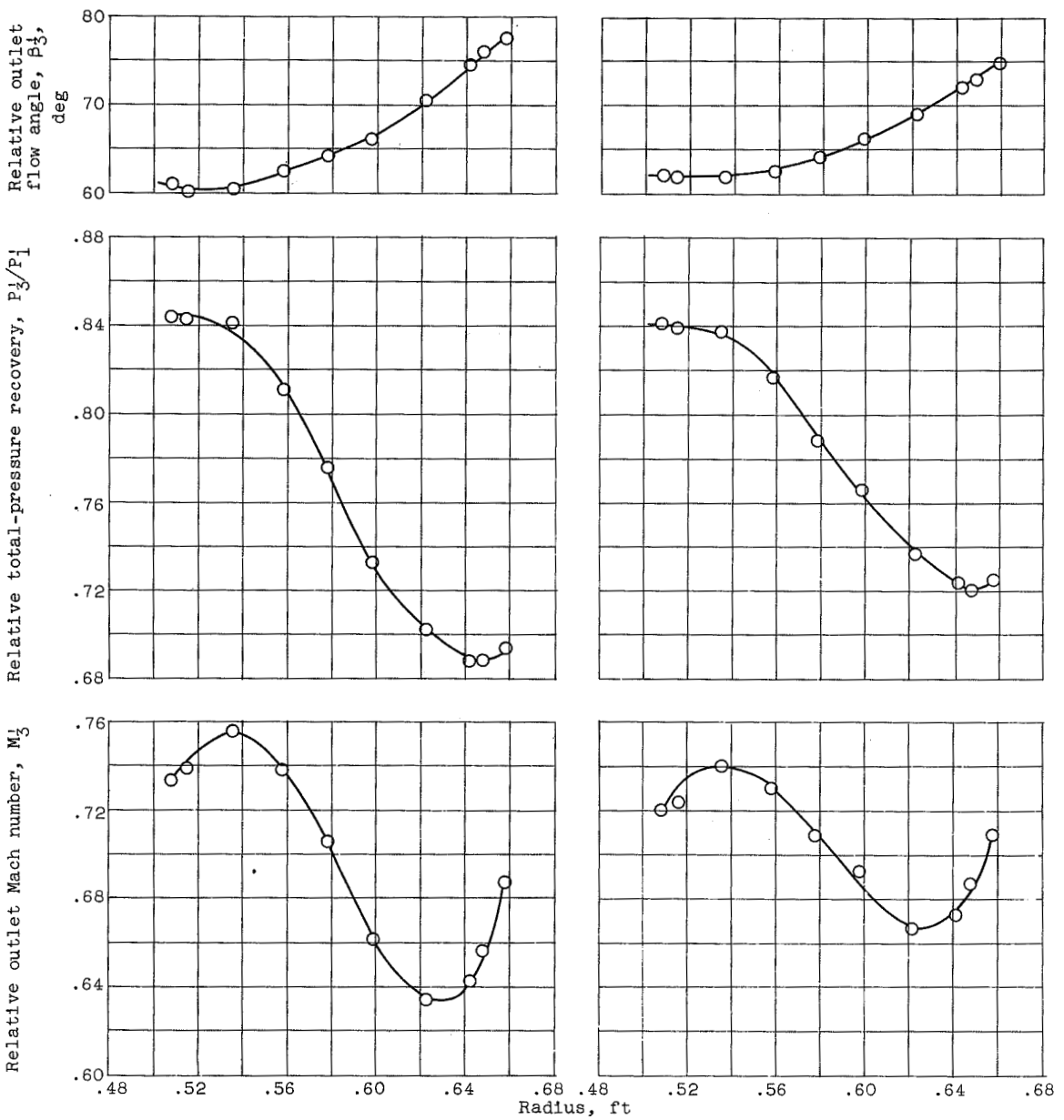

(a) Original rotor. (b) Modified rotor.

Figure 10. - Relative outlet conditions for original and modified external-compression rotors at design speed and maximum pressure ratio at maximum weight flow (points A and B of fig. 7).

[redacted]

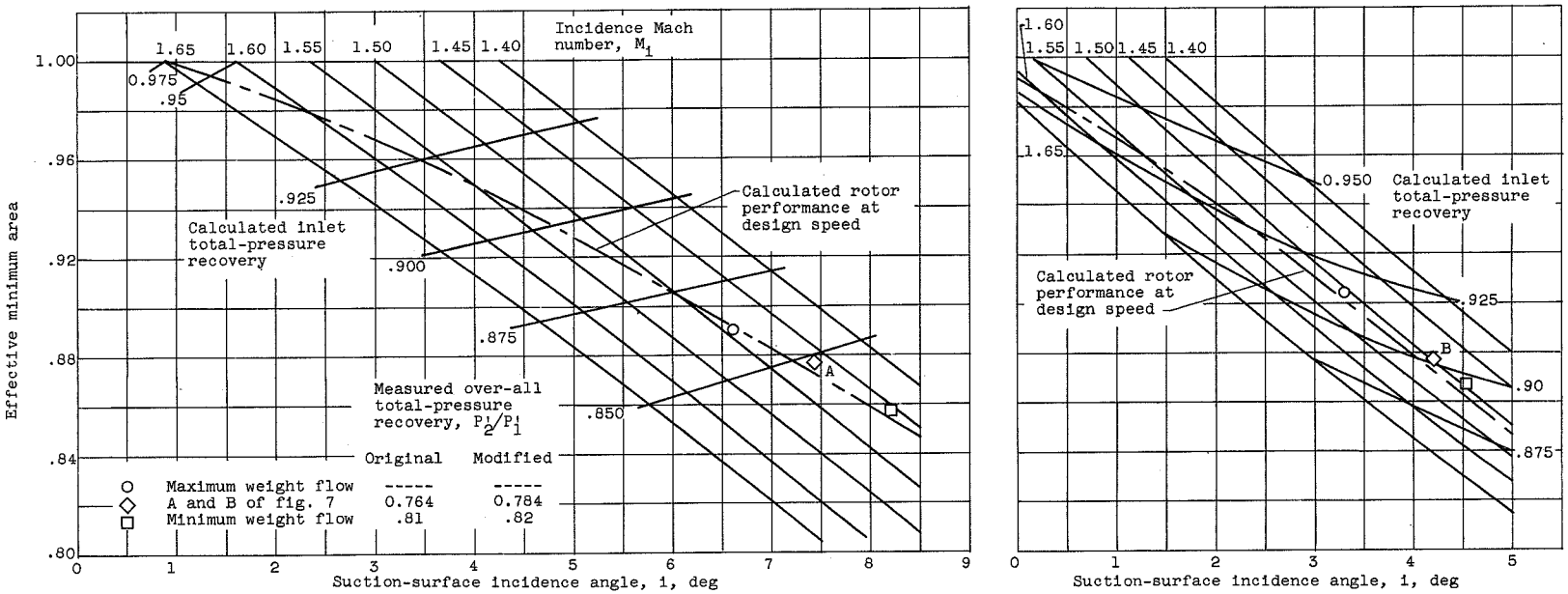

(a) Original rotor.

(b) Modified rotor.

Figure 11. - Calculated inlet performance for original and modified 16-inch external-compression supersonic-compressor rotor cascades at pitch section.

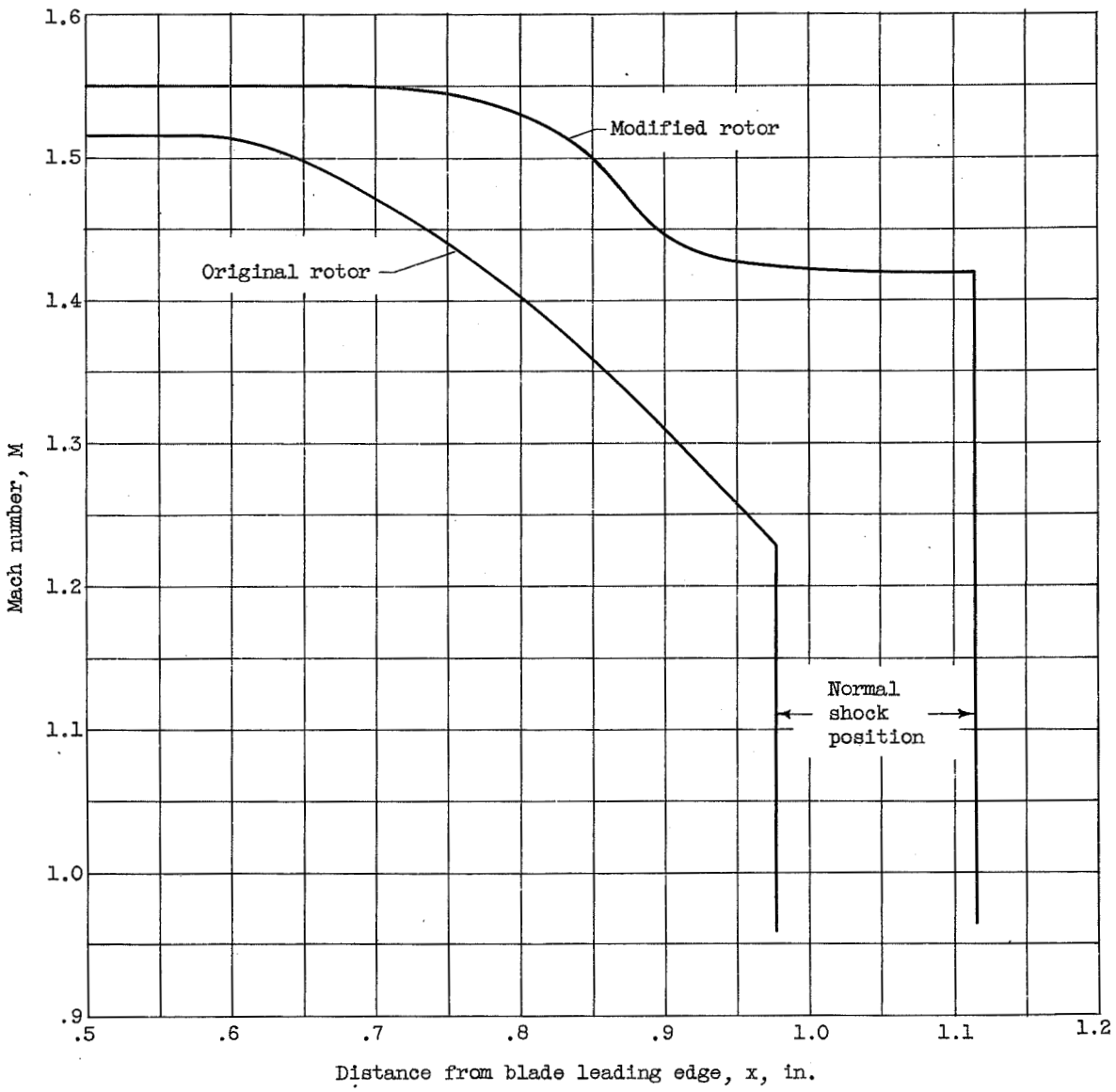

Figure 12. - Mach number gradient near suction surface of original and modified external-compression supersonic-compressor rotor with inlet conditions at maximum pressure ratio at maximum weight-flow points (points A and B of fig. 7).

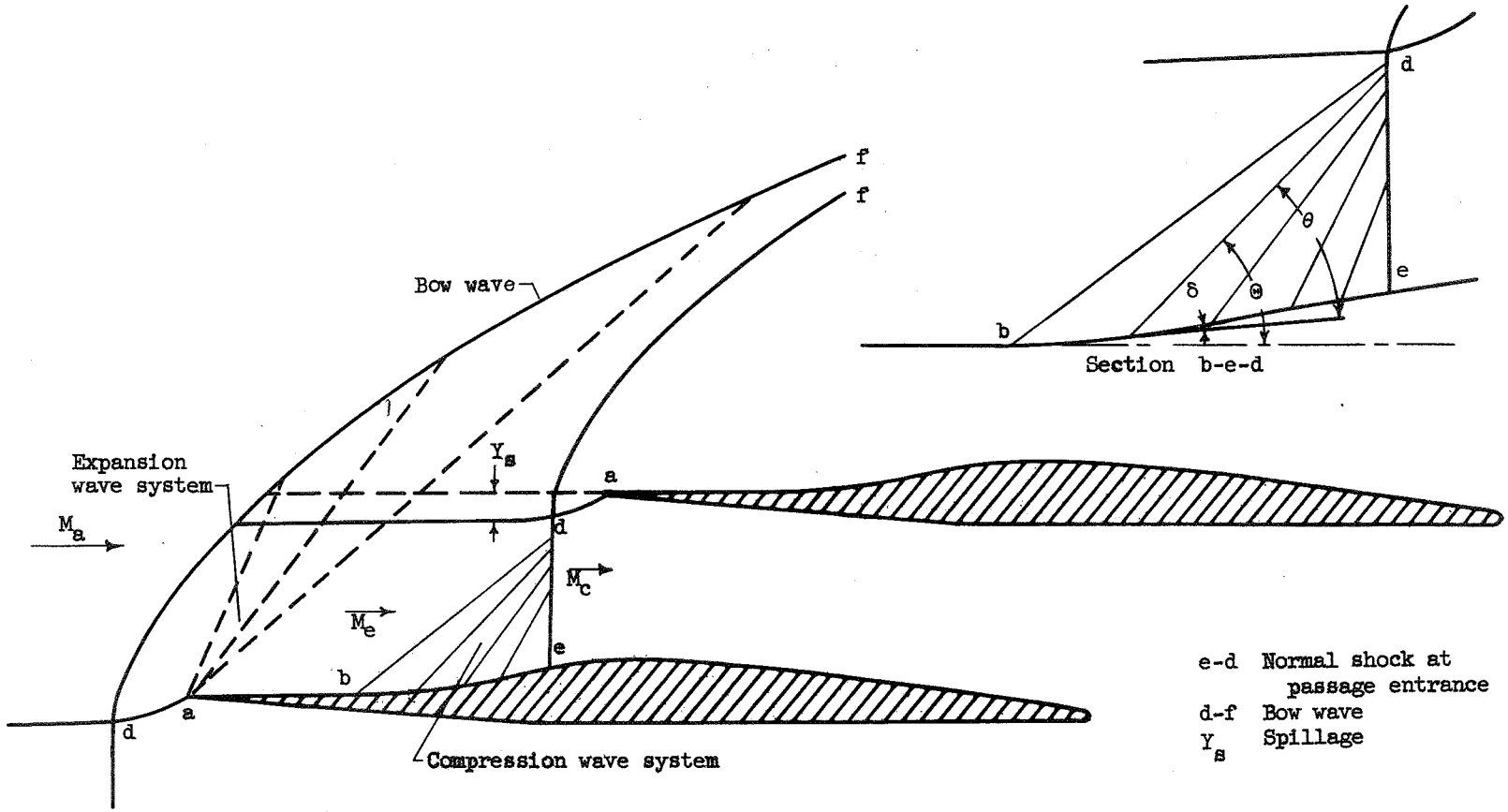

Figure 13. - Sketch of off-design performance configuration as used for computation of entrance section losses for original 16-inch external-compression supersonic-compressor rotor.

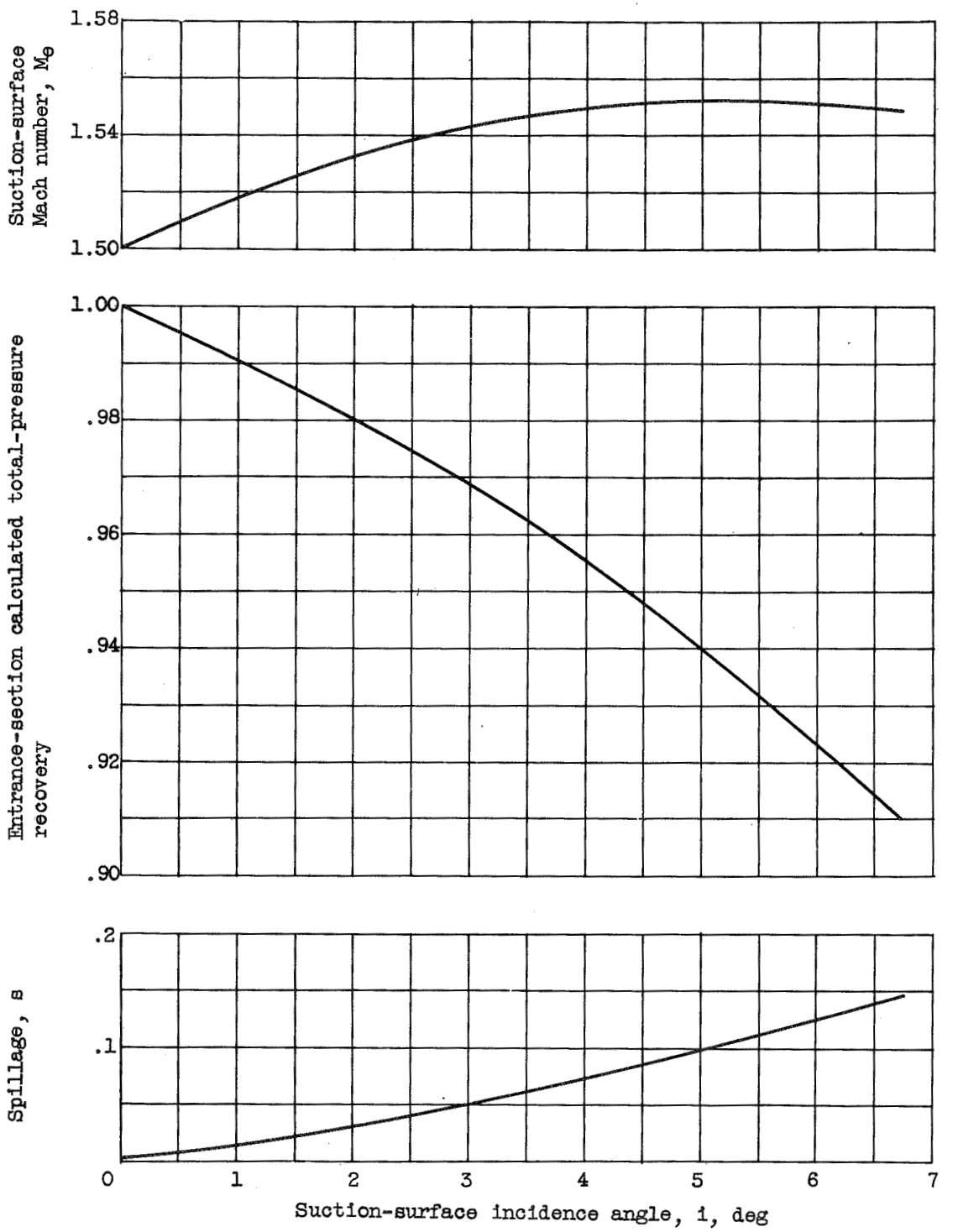

Figure 14. - Computed conditions for bow wave over range of suction-surface incidence angle for original 16-inch external-compression supersonic-compressor rotor. Inlet Mach number, 1.5; design entrance flow angle, 63.35°.

[redacted]

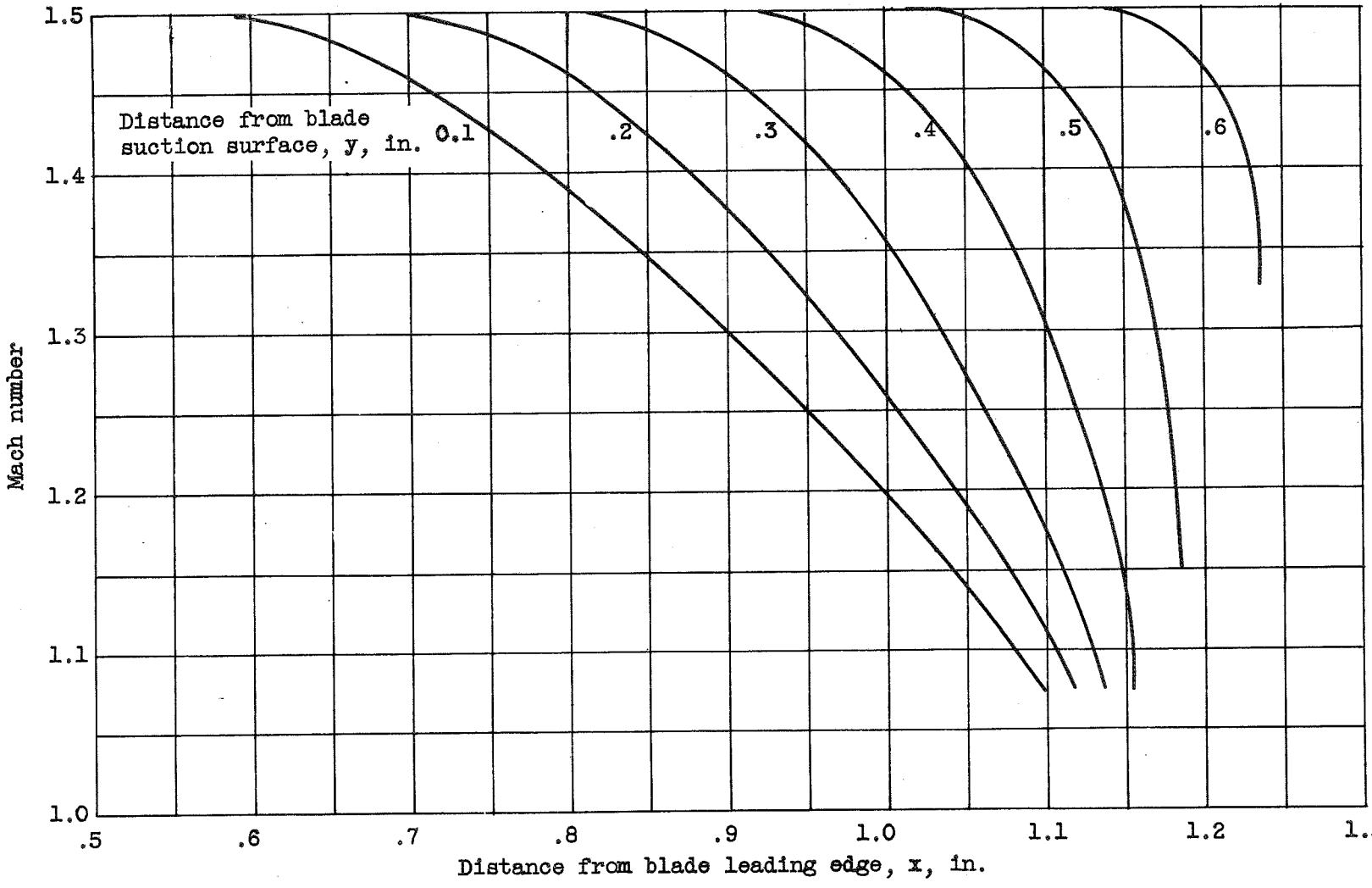

Figure 15. - Mach number distribution near entrance section of original rotor blade profile. Suction-surface Mach number, 1.5.

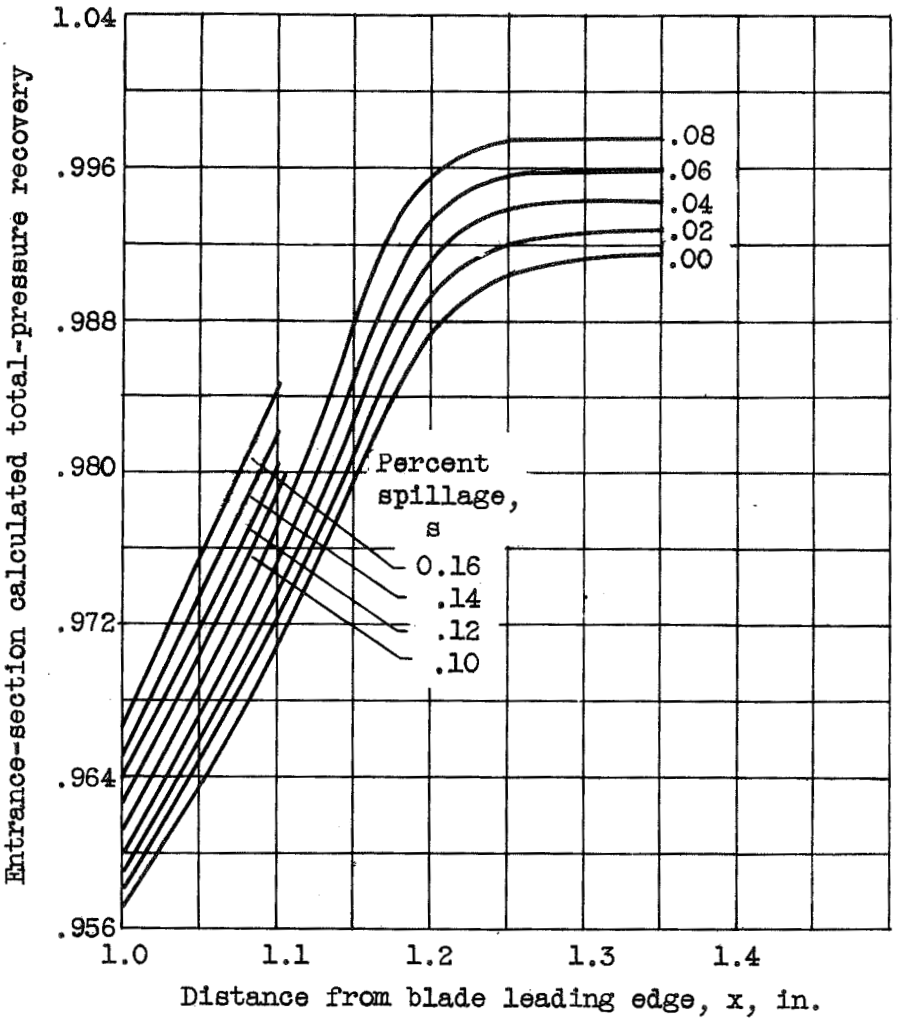

Figure 16. - Variation in calculated normal-shock total-pressure recovery at entrance section of 16-inch external-compression supersonic-compressor rotor. Suction-surface Mach number, 1.5.

NACA-Langley - 9-24-54 - 350